ISSN 0915-633X

NATIONAL INSTITUTE FOR FUSION SCIENCE

Stabilization of Kinetic Internal Kink Mode by Ion Diamagnetic Effects

H. Naitou, T. Kuramoto, T. Kobayashi, M. Yagi,
S. Tokuda and T. Matsumoto

(Received - Feb. 21, 2000)

NIFS-635 Apr. 2000

RESEARCH REPORT
NIFS Series

NAGOYA, JAPAN

Stabilization of Kinetic Internal Kink Mode by Ion Diamagnetic Effects

H. Naitou*, T. Kuramoto, T. Kobayashi[1],
M. Yagi[2], S. Tokuda[3] and T. Matsumoto[3]

Department of Electrical and Electronic Engineering,
Yamaguchi University, Tokiwadai 2-16-1, Ube 755-8611, Japan
[1] Integrated Information Processing Center,
Yamaguchi University, Tokiwadai 2-16-1, Ube 755-8611, Japan
[2] Research Institute for Applied Mechanics, Kyushu University, Kasuga 816, Japan
[3] Department of Fusion Plasma Research, Naka Fusion Research Establishment,
Japan Atomic Energy Research Institute, Naka Ibaraki 311-0193, Japan

Abstract

Ion diamagnetic effects on the $m = 1$ (poloidal mode number) and $n = 1$ (toroidal mode number) kinetic internal kink mode are studied numerically by the three-field gyro-reduced-MHD code in the cylindrical coordinates, GRM3F-CY. In the derivation of the gyro-reduced-MHD model including the ion diamagnetic effects, finite gyroradius effects of ions are added to the gyrokintic Poisson equation (quasi-neutral condition) and the convection term of the conservation law of the ion density. It is found that the long wavelength approximation, $k_\perp \rho_{ti} \ll 1$, where $k_\perp$ is the wavenumber perpendicular to the magnetic field and ρ_{ti} is the thermal ion gyroradius, fails to reproduce the correct dispersion relation; the formulation valid even for $k_\perp \rho_{ti} \gg 1$ is necessary. The results of numerical calculation coincide with the theory for $|\omega_{*e}| + |\omega_{*i}| < 2\gamma_0$, where the growth rate reduces as the density gradient increases. Here ω_{*e} and ω_{*i} are electron and ion diamagnetic angular frequencies estimated at the rational surface of $q = 1$ (q is a safety factor), respectively, and γ_0 is the growth rate for the uniform density. Very weak instability, however, is observed for $|\omega_{*e}| + |\omega_{*i}| > 2\gamma_0$, where the theory predicts the complete stabilization. This residual instability appears since the region with the density gradient is limited in the radial direction and the stabilization by the outgoing drift-wave like mode becomes incomplete.

Keywords: tokamak, internal kink mode, gyrokinetic theory, kinetic effect, diamagnetic effect, gyro-fluid model, gyro-reduced-MHD model

1 Introduction

To reproduce the kinetic magnetohydrodynamic (MHD) phenomena in tokamaks by the numerical simulation technique is a challenging project. In present day and future high temperature large tokamaks, it is not and it will be not unusual that the standard ideal and resistive MHD models fail to explain the phenomena observed experimentally. The inertia of electrons, diamagnetic effects of electrons and ions, finite gyroradius effects of ions, and the Landau damping are examples of the kinetic effects which can significantly modify the MHD phenomena. Those kind of kinetic effects can be included by the gyrokinetic particle, gyrofluid, gyro-reduced-MHD, and hybrid simulations. It is important to develop several codes with different orders of physical accuracy and to benchmark those codes for the same physical phenomena.

We have developed the gyrokinetic particle code (GYR3D)[1, 2, 3], the gyro-reduced-MHD code (GRM3D-2F)[4, 5], and the hybrid code (Hybrid3D)[6] to study kinetic modification of MHD modes. These codes have been coded for the rectangular mesh and fast Fourier transformation technique is used. The linear and nonlinear development of the $m = 1$ (poloidal mode number) and $n = 1$ (toroidal mode number) kinetic internal kink mode are simulated successfully. Fast full reconnection followed by a second phase in which the configuration with $q_0 < 1$ (q_0 is the safety factor at the magnetic axis) is reformed has been observed by these three codes. However it has been felt that the cylindrical model with mode expansions in toroidal and poloidal angles would be more powerful to simulate realistic plasmas. The mesh accumulation technique in the radial direction can be used for the cylindrical code. For example, in order to simulate an $m = 1$ and $n = 1$ kinetic internal kink mode, we must resolve the fine mode structure of the current perturbation around the $q = 1$ magnetic

*Guest staff of National Institute for Fusion Science, Toki, Gifu 509-5292, Japan (April 1, 1999 - March 31, 2001)

surface with the characteristic length of the collisionless electron skin depth, $d_e = c/\omega_{pe}$ (c is the speed of light in vacuum and ω_{pe} is the electron plasma angular frequency). For the parameters of present day large tokamaks, d_e/a (a is a minor radius of a plasma) is less than 10^{-3}. By accumulating radial meshes around the $q = 1$ surface, we can simulate the physics including the thin inertial layer by using the moderate number of meshes.

As the first step to build the series of cylindrical codes, we developed linear version of the GRM3F-CY code which is based on the three field gyro-reduced-MHD model. The stabilization of the kinetic internal kink mode by the electron diamagnetic effect was studied by Naitou et al. [7] using the three field gyro-reduced-MHD model in the limit of $T_i = 0$ (T_i is the ion temperature). The most important finding was that the stabilization of the internal kink mode by the electron diamagnetic effects is not clearly observed for the simulation of $d_e/a \simeq 10^{-1} - 10^{-2}$. The simulation with $d_e/a < 10^{-3}$ verified the stabilization of the mode and the existence of the very weak instability for the large density gradient in which theories [8, 9, 10, 11] predict the complete stabilization. Hence the simulation with $d_e/a < 10^{-3}$ has much reality to compare with actual experiments. This paper extends the work of the previous paper[7] and investigates the diamagnetic effects of ions on the kinetic internal kink mode using the realistic parameter of d_e/a.

The outline of the paper is as follows. The basic formulation of the gyro-reduced-MHD model with the finite gyroradius effects of ions are summarized in Sec. 2. Simulation model is described in Sec.3. Section 4 shows results of linear mode analysis by the GRM3F-CY code with the finite gyroradius effects of ions. The conclusions and discussion are given in Sec.5.

2 Basic Equations

The five field gyro-reduced MHD model [12] was derived by moment equations of the gyrokinetic Vlasov-Maxwell system [13]. The name of gyro-reduced-MHD comes from the fact that the basic equations are the gyrokinetic generalization of the two field reduced MHD model by Strauss [14]. Not all of the finite gyroradius effects of ions were included in the Lee's formulation; hence, this article aims the improvement of the gyro-reduced-MHD model. By assuming $\Gamma_i = 0$ (ion flux along the magnetic field), the five field model reduces to the three field model which is equivalent to the subset of the four field model (in the limit of $T_i = 0$) given by Aydemir [15]. The four field model by Aydemir is the simplified version of the four field model by Hazeltine et al. [16] which is based on the Vlasov-Maxwell system. When the ion gyroradius effects are included, the relation between the Hazeltine's four field model and the treatment based on the gyrokinetic formulation is not clear. We believe that this article bridges some of the gaps between the Hazeltine's four field model and the gyro-reduced-MHD formulation.

Here we derive the three field gyro-reduced-MHD model with kinetic modifications from the gyrokinetic Vlasov-Maxwell system given by Hahm [13]. The gyrokinetic equations are derived using the ordering of

$$\begin{aligned} \frac{\omega}{\omega_{ci}} \simeq \frac{\rho_{ti}}{L} \simeq \frac{k_\parallel}{k_\perp} &\simeq \frac{e\phi}{T_e} \simeq \frac{\delta B}{B} \simeq O(\epsilon)\,, \\ k_\perp \rho_{ti} &\simeq O(1)\,, \end{aligned} \tag{1}$$

where ω is the characteristic mode frequency, ω_{ci} is the ion cyclotron frequency, ρ_{ti} is the thermal ion gyroradius, L is the characteristic length of the gradient of the macroscopic quantities like density, temperature, and magnetic field, and $k_\parallel$ and $k_\perp$ are the wave numbers parallel and perpendicular to the magnetic field, respectively, e is the electron charge, ϕ is the electrostatic potential, T_e is the electron temperature, δB is the variation of the magnetic field from a constant longitudinal magnetic field B, and ϵ is the smallness parameter. This ordering is valid for the low frequency phenomena in the bulk plasma in tokamaks.

We assume a uniform (toroidal) magnetic field, $\boldsymbol{B} = B_0 \boldsymbol{b}$, where $\boldsymbol{b}$ is the unit vector in the z direction. The (poloidal) magnetic field in the x, y plane is expressed by $\boldsymbol{\nabla} \times (A_z \boldsymbol{b}) = \boldsymbol{\nabla} A_z \times \boldsymbol{b}$ with A_z being the z component of the vector potential. The compressional component of the toroidal magnetic field is neglected in the low-β approximation. The electric field consists of the electrostatic component, $-\boldsymbol{\nabla}\phi$, and the induced electric field along the magnetic field, $-\partial A_z/\partial t$.

The gyrokinetic Vlasov equation for the electron distribution function $f_e(\boldsymbol{r}, v_\parallel, t)$ with $\boldsymbol{r}, v_\parallel$, and t being the coordinates of the configuration space, the velocity along the magnetic field, and the time, respectively, is given by

$$\begin{aligned} \frac{\partial f_e}{\partial t} &+ \left(v_\parallel \boldsymbol{b}^* + \frac{\boldsymbol{b} \times \nabla \phi}{B_0} \right) \cdot \boldsymbol{\nabla} f_e \\ &- \frac{e}{m_e} \left(-\boldsymbol{b}^* \cdot \nabla \phi - \frac{\partial A_z}{\partial t} \right) \frac{\partial f_e}{\partial v_\parallel} = 0\,, \end{aligned} \tag{2}$$

where m_e is the electron mass and $\boldsymbol{b}^*$ is the unit vector of the magnetic field,

$$\boldsymbol{b}^* = \boldsymbol{b} + \frac{\nabla A_z \times \boldsymbol{b}}{B_0}\,. \tag{3}$$

While the electron finite gyroradius effect is neglected because of small mass, the ion gyroradius effect is included to the gyrokinetic Vlasov equation for the ion velocity distribution function $f_i(\boldsymbol{r}, v_\parallel, v_\perp, t)$:

$$\begin{aligned} &\frac{\partial f_i}{\partial t} + \left[v_\parallel \boldsymbol{b}^* + \frac{\boldsymbol{b} \times \boldsymbol{\nabla}(J_0 \phi)}{B_0} \right] \cdot \boldsymbol{\nabla} f_i \\ &+ \frac{q_i}{m_i} \left[-\boldsymbol{b}^* \cdot \boldsymbol{\nabla}(J_0 \phi) - \frac{\partial (J_0 A_z)}{\partial t} \right] \frac{\partial f_i}{\partial v_\parallel} = 0\,, \end{aligned} \tag{4}$$

where q_i is the ion charge, m_i the ion mass, and J_0 the linear operator which carries out the gyroaveraging operation. In Fourier space, J_0 is a Bessel function with an argument of $k_\perp \rho_i$, where $\rho_i = v_\perp/\omega_{ci}$

is the ion gyroradius and $v_\perp$ the velocity perpendicular to the magnetic field. It is to be noted that in the gyrokinetic theory f_i denotes the velocity distribution for guiding centers. Also the ion polarization response is not included in f_i.

In order to calculate the fields ϕ and A_z, the zeroth and first order moments of f_e and f_i are needed. The zeroth order moments of f_e and f_i determine the electron and ion densities, n_e and $< n_i >$, respectively,

$$n_e(\boldsymbol{r},t) = \int dv_\parallel f_e(\boldsymbol{r},v_\parallel,t)\,, \tag{5}$$

$$< N_i(\boldsymbol{r},t) > = \int d(2\pi v_\perp) dv_\parallel J_0 f_i(\boldsymbol{r}.v_\parallel,v_\perp,t)\,, \tag{6}$$

where angular brackets indicate the gyro-averaging. Note that $< N_i >$ designates the particle density, while N_i,

$$N_i(\boldsymbol{r},t) = \int d(2\pi v_\perp) dv_\parallel f_i(\boldsymbol{r},v_\parallel,v_\perp,t)\,, \tag{7}$$

is the guiding center density. The first order moment of f_e determines the electron current along the magnetic field which is given by the following equation.

$$J_e(\boldsymbol{r},t) = -en_e(\boldsymbol{r},t)v_e(\boldsymbol{r},t) = -e\int dv_\parallel v_\parallel f_e(\boldsymbol{r},v_\parallel,t)\,, \tag{8}$$

where v_e is the electron fluid velocity along the magnetic field. We assume that ion current along the magnetic field is zero; hence the coupling to ion sound wave is neglected.

The electrostatic potential is given by the gyrokinetic Poisson equation,

$$-\frac{T_e}{T_i\lambda_{De}^2}(1-\Gamma_0)\phi = \frac{1}{\epsilon_0}(en_e - q_i < N_i >)\,, \tag{9}$$

where ϵ_0 is the permittivity of vacuum, λ_{D_e} is the electron Debye length estimated by the average density, and Γ_0 is the real space operator which corresponds to $\Gamma_0(k_\perp^2\rho_{ti}^2) = I_0(k_\perp^2\rho_{ti}^2)\exp(-k_\perp^2\rho_{ti}^2)$ in Fourier space (I_0 is the modified Bessel function). The real ion density n_i is obtained by adding the ion polarization response to $< N_i >$;

$$n_i =< N_i > -\frac{\epsilon_0 T_e}{q_i T_i \lambda_{De}^2}(1-\Gamma_0)\phi\,. \tag{10}$$

Hence, the gyrokinetic Poisson equation is equivalent to the quasi-neutrality condition, $n_e = n_i$. In the long wavelength limit the left hand side of Eq.(9) becomes $(\omega_{pi}^2/\omega_{ci}^2)\nabla_\perp^2\phi$ where $q_i = e$ is assumed, ω_{pi} is the ion plasma frequency, and $\nabla_\perp^2$ is the Laplacian operator perpendicular to the magnetic field.

Ampere's law determines A_z:

$$\nabla_\perp^2 A_z = -\mu_0 J_e\,, \tag{11}$$

where μ_0 is the vacuum permeability. Equations (2), (4), (5), (6), (8), (9), and (11) give the closed set of gyrokinetic Vlasov-Maxwell system.

The gyro-reduced-MHD model is derived by the two-fluid gyrofluid model which is based on the moment equations of the gyrokinetic Vlasov equations. Although, the Landau damping and higher order moments can be taken into account in the gyrofluid model, we are only interested in the lower order moments.

The equation for the conservation of electron density is obtained by integrating Eq.(2) over $v_\parallel$:

$$\frac{dn_e}{dt} + \boldsymbol{b}^*\cdot\boldsymbol{\nabla}(n_e v_e) = 0\,, \tag{12}$$

where d/dt is the convective derivative defined by

$$\frac{d}{dt} = \frac{\partial}{\partial t} + \frac{\boldsymbol{b}\times\boldsymbol{\nabla}\phi}{B_0}\cdot\boldsymbol{\nabla}\,. \tag{13}$$

The conservation law for the ion density,

$$\frac{d< N_i >}{dt} + (\Gamma_0 - 1)\frac{\boldsymbol{b}\times\boldsymbol{\nabla}\phi}{B_0}\cdot\boldsymbol{\nabla}N_i = 0\,, \tag{14}$$

is derived by integrating Eq.(4) over $v_\parallel$ and $v_\perp$ after multiplying $2\pi v_\perp J_0$. The dominant term for the gyro-averaged $\boldsymbol{E}\times\boldsymbol{B}$ drift is kept as in the paper by Dorland and Hammett[17]. The second term in the left hand side of the equation indicates the deviation of the gyroaveraged $\boldsymbol{E}\times\boldsymbol{B}$ drifts from the simple estimation neglecting the finite gyroradius effect, $\boldsymbol{b}\times\boldsymbol{\nabla}\phi/B_0$.

The first moment equation for electrons is given by the following equation.

$$\frac{dJ_e}{dt} - \frac{eT_e}{m_e}\boldsymbol{b}^*\cdot\boldsymbol{\nabla}n_e = \frac{n_{e0}e^2}{m_e}\left(-\boldsymbol{b}^*\cdot\boldsymbol{\nabla}\phi - \frac{\partial A_z}{\partial t}\right)\,, \tag{15}$$

where higher order nonlinear term is neglected, n_e in the right hand side of the equation is replaced by n_{e0} (Boussinesq like approximation [18]), and isothermal model (T_e = constant) is used to evaluate electron pressure along the magnetic field.

Oerating d/dt on the gyrokinetic Poisson equation (Eq.(9)), replacing dn_e/dt and dn_i/dt by Eqs.(12) and(14), and using Ampere's law (Eq.(11)) we have the vortex equation;

$$-\frac{1}{\rho_{ti}^2}\frac{d}{dt}[(1-\Gamma_0)\phi] = -v_A^2\boldsymbol{b}^*\cdot\boldsymbol{\nabla}(\nabla_\perp^2 A_z) + \frac{T_i}{en_{e0}}\frac{1-\Gamma_0}{\rho_{ti}^2}\frac{\boldsymbol{b}\times\boldsymbol{\nabla}\phi}{B_0}\cdot\boldsymbol{\nabla}N_i\,. \tag{16}$$

where $v_A = c\omega_{ci}/\omega_{pi}$ is the Alfvén velocity. The second term on the right hand side of the equation indicates the variation of the charge density caused by the difference in the $\boldsymbol{E}\times\boldsymbol{B}$ drifts of electrons and ions.

Generalized Ohm's law along the magnetic field is nothing but the first order momentum equation of electrons along the magnetic field (Eq (15));

$$\frac{\partial A_z}{\partial t} = -\boldsymbol{b}^*\cdot\nabla\phi + d_e^2\frac{d}{dt}(\nabla_\perp^2 A_z) + \frac{T_e}{en_{e0}}\boldsymbol{b}^*\cdot\nabla n_e\,, \tag{17}$$

where Ampere's law, Eq.(11), is used to eliminate J_z in the expression. The electron diamagnetic effect originates from the third term on the right hand side of the equation.

The equation for the conservation of electrons (Eq.(12)) is modified by using Ampere's law (Eq.(11));

$$\frac{dn_e}{dt} = -\frac{1}{e\mu_0}\boldsymbol{b}^* \cdot \nabla(\nabla_\perp^2 A_z) . \tag{18}$$

In addition to these three equations of (16), (17), and (18), the conservation law of ions which describes the time variation of the ion density will complete the closed set of equations. In this paper, we are interested in the linear analysis. In the linear treatment, N_i in the vortex equation represents the equilibrium quantity; hence, the coupling to the conservation law of ions can be neglected.

For the uniform density and the uniform magnetic field, the angular frequency of the normal mode is given by linearizing Eqs.(16), (17), and (18),

$$\omega^2 = \frac{k_\parallel^2 v_A^2}{1+k_\perp^2 d_e^2}\left[\frac{k_\perp^2\rho_i^2}{1-\Gamma_0(k_\perp^2\rho_i^2)} + k_\perp^2\rho_s^2\right] \tag{19}$$

which is the angular frequency of the kinetic Alfvén wave [19].

Here, we make some discussions about the vortex equation. In the long wavelength limit, we can approximate $1-\Gamma_0$ as $-\rho_{ti}^2\nabla_\perp^2$. Hence the vortex equation in the long wavelength limit is given by

$$\begin{aligned}\frac{d}{dt}(\nabla_\perp^2\phi) &= -v_A^2\boldsymbol{b}^*\cdot\nabla(\nabla_\perp^2 A_z) \\ &+ \frac{T_i}{en_{e0}}\frac{\boldsymbol{b}\times\boldsymbol{\nabla}N_i}{B_0}\cdot\boldsymbol{\nabla}(\nabla_\perp^2\phi) ,\end{aligned} \tag{20}$$

where the ion diamagnetic drift velocity,

$$\boldsymbol{v}_{*i} = \frac{T_i}{en_{e0}}\frac{\boldsymbol{b}\times\boldsymbol{\nabla}N_i}{B_0} , \tag{21}$$

is included in the second term on the right hand side of the equation. Equation (20) is first derived by Hasegawa and Wakatani [20] for their proposal of finite-Larmor radius magnetohydrodynamic equations for microturbulence. It will be found in the following section that the correct dispersion relation for the kinetic internal kink mode is not reproduced using Eq.(20).

In the limit of $T_i = 0$, with Eqs.(17) and (18), the vortex equation, Eq.(20), constitutes the closed set of the three field gyro-reduced-MHD model which was used in the previous paper [7] to study the electron diamagnetic effects on the kinetic internal kink mode. For the case of uniform equilibrium density, replacing n_e in Eq.(17) by $(\epsilon_0/e)(\omega_{pe}^2/\omega_{ce}^2)$ using the long wavelength limit of the gyrokinetic Poisson equation, Eq.(9), the generalized Ohm's law becomes

$$\frac{\partial A_z}{\partial t} = -\boldsymbol{b}^*\cdot\nabla\phi + d_e^2\frac{d}{dt}(\nabla_\perp^2 A_z) + \rho_s^2\boldsymbol{b}^*\cdot\nabla(\nabla_\perp^2\phi), \tag{22}$$

where $\rho_s = \sqrt{T_e/m_i}/\omega_{ci}$ is the thermal ion gyroradius estimated by the electron temperature. Equation (20) with $T_i = 0$ and Eq.(22) make the two field gyro-reduced-MHD model used in the papers [4, 5].

When $T_i \neq 0$, it is important to include the ion response which is valid even for $k_\perp\rho_{ti} \gg 1$ because ρ_{ti} is much larger than d_e and near the rational surface the resolution of the mode structure with the scale length of d_e is crucial. Hence, we make the Padé like approximation for Γ_0 which is expressed in Fourier space as

$$1-\Gamma_0(k_\perp^2\rho_{ti}^2) \cong \frac{k_\perp^2\rho_{ti}^2}{1+k_\perp^2\rho_{ti}^2} . \tag{23}$$

The above approximation is rigorously correct through second order in $k_\perp\rho_{ti}$ while still being well behaved for large $k_\perp\rho_{ti}$ [21]. We can use Fourier transformation technique to numerically execute above operation. However, we are using the code with nonuniform radial mesh because mesh accumulation is needed to represents the fine mode structure around the rational surface. Hence we stick to the finite difference method without Fourier transformation. For this purpose, we multiply $1+k_\perp^2\rho_{ti}^2$ to the both sides of the vortex equation. We have the vortex equation valid for the whole region of $k_\perp\rho_{ti}$;

$$\begin{aligned}\frac{d}{dt}(\nabla_\perp^2\phi) &= v_A^2(1-\rho_{ti}^2\nabla_\perp^2)\boldsymbol{b}^*\cdot\boldsymbol{\nabla}(\nabla_\perp^2 A_z) \\ &+ \frac{T_i}{en_{e0}}\frac{\boldsymbol{b}\times\boldsymbol{\nabla}N_i}{B_0}\cdot\boldsymbol{\nabla}(\nabla_\perp^2\phi) .\end{aligned} \tag{24}$$

If, in the Aydemir's four field model, the vortex equation for the generalized vorticity is rearranged using the conservation law of the electron density, the resultant vortex equation for $\nabla_\perp^2\phi$ is very close to Eq.(24). Equations (17), (18), and (24) form the basic equations for the linerized version of GRM3F-CY code with finite gyroradius effects of ions.

3 Simulation Model

We assume a cylinder with a minor radius of a and a height of $L_z = 2\pi R$ (R is a major radius) surrounded by a perfectly conducting wall. Periodic boundary condition is used in the z direction. GRM3F-CY utilizes the following normalization: $z/L_z \to z$, $r/a \to r$, $tv_A/L_z \to t$, $A_z L_z/(a^2 B_0) \to A_z$, $\phi L_z/(v_A a^2 B_0) \to \phi$, $n_e L_z/(n_{e0} d_e) \to n_e$, $n_i L_z/(n_{e0} d_e) \to n_i$. The normalized equations include only three parameters, d_e/a, ρ_s/a, and $\rho_i/a = \sqrt{T_i/T_e}\rho_s/a$.

We selected the parameters close to the present day large tokamaks: $a = 1$ [m], $R = 3$ [m], $n_{e0} = 10^{20}$ [m^{-3}], magnetic field strength of $B = 5$ [Tesla], and $T_e = 10$ [kev]. For such a tokamak with deuterium discharge, $d_e/a = 5.315\times10^{-4}$ and $\rho_s/a = 2.891\times10^{-3}$. The profile of the safety factor is

$$q(r) = q_0\left[1-4(1-q_0)\left(\frac{r}{a}\right)^2\right]^{-1} , \tag{25}$$

where $q_0 = 0.85$ is the safety factor at the magnetic axis. Note that $q(a/2) = 1.0$ and $q(a) = 2.125$. The equilibrium density profile is chosen as

$$n(r) = n_0\left(1-\epsilon_n\tanh\frac{r-r_0}{l_n}\right) , \tag{26}$$

where $r_0 = a/2$, $l_n = 0.16a$, and ϵ_n is used to change the density gradients

Since we are doing the linear analysis, only a mode of $m = 1$ and $n = 1$ is needed. So the linear equations have the form of finite difference equations in the radial coordinate and the time. The density profile of the nonuniform radial mesh is given by the following equation,

$$g(r) = p_0 + \sum_{n=1}^{N} p_n \frac{1}{a_n} \frac{\mathrm{sech}^2 \frac{r-r_n}{a_n}}{\tanh \frac{1-r_n}{a_n} - \tanh \frac{-r_n}{a_n}} , \quad (27)$$

where r is the normalized radius and $p_0+p_1+\cdots+p_N = 1$. While p_0 shows the ratio for the uniform part of the mesh, p_n represents the ratio for the part of the accumulated mesh with the center position r_n and the width a_n. Here we employed the multiple mesh accumulations at the rational surface of $q = 1$. For the uniform mesh 40 per cents of the number of meshes are used, $p_0 = 0.4$. We have selected $N = 3$. The mode structure with the characteristic length of d_e is resolved by the accumulated mesh of $n = 1$ with $p_1 = 0.3$ and $a_1 = 0.00075$. The mode structure with the characteristic lengths of ρ_s and ρ_i is represented by the accumulated mesh of $n = 2$ with $p_2 = 0.15$ and $a_2 = 0.006$. The third mesh accumulation is needed to mitigate the sharp change in the mesh density from the uniform mesh to the accumulated mesh of $n = 2$; for $n = 3$, $p_3 = 0.15$ and $a_3 = 0.032$.

4 Simulation Results

The effects of the density gradient on the stability of the $m = 1$ and $n = 1$ kinetic internal kink mode is studied by the linearized version of GRM3F-CY code which simulates the time evolution of the unstable mode as a initial value problem. Electron diamagnetic effects are studied in the previous article[7]. Ion diamagnetic effects is added to the previous model which included only electron diamagnetic effects. When $T_i/T_e = 0$, the new model includes only electron diamagnetic effects. Two parameters of T_i/T_e and ϵ_n which determine the magnitude of the density gradient, are key parameters.

Figure 1 shows the measured growth rates depending on the magnitudes of the density gradient. The case of $T_i/T_e = 1.0$ is shown. The electron and ion diamagnetic frequencies which are estimated at the rational surface of $q = 1$ are defined by $\omega_{*e} = -(T_e/reB_0n_e)dn_e/dr$ and $\omega_{*i} = (T_i/reB_0n_i)dn_i/dr$, respectively. In this article, the electron diamagnetic frequency is expressed with negative value, while the ion diamagnetic frequency is designated by the positive value. We have used 256 nonuniform grid points in the radial direction. The meshes are accumulated at the rational surface of $q = 1$ located at $r = 0.5a$. The measured growth rate for the uniform density is $\gamma_0 = 7.19 \times 10^{-3} v_A/L_z$ which agrees very well with the theoretical value of $\gamma_0 = 9.19 \times 10^{-3} v_A/L_z$ (see Eq.(29)). The measured characteristic time for the instability, $1/\gamma_0$, is about 340 μsec.

The theoretical curve written in the figure is obtained from the dispersion relation which is given by the following equation [8, 9, 10, 11].

$$(\omega - \omega_{*e})^3(\omega - \omega_{*i})^3 = (i\gamma_0)^6 , \quad (28)$$

Here, γ_0 is the growth rate without the density gradient which is given by, for $\rho_s \gg d_e$,

$$\gamma_0 = 2\pi q'(d_e)^{1/3}(\rho_s^2 + \rho_i^2)^{1/3} \frac{v_A}{L_z} . \quad (29)$$

where $q' = dq/dr$ represents the magnetic shear estimated at the rational surface of $q = 1$. The solution of the above dispersion relation, $\omega = \omega_r + i\gamma$, is for the small density gradient of $|\omega_{*e}| + |\omega_{*i}| \le 2\gamma_0$,

$$\omega_r = \frac{\omega_{*e} + \omega_{*i}}{2} , \quad (30)$$

$$\gamma = \gamma_0 \sqrt{1 - (\omega_{*e} - \omega_{*i})^2/(2\gamma_0)^2} , \quad (31)$$

and for the large density gradient of $|\omega_{*e}|+|\omega_{*i}| > 2\gamma_0$,

$$\omega_r = \frac{\omega_{*e} + \omega_{*i}}{2} \pm \frac{\sqrt{(\omega_{*e} - \omega_{*i})^2 - 4\gamma_0^2}}{2} , \quad (32)$$

$$\gamma = 0 . \quad (33)$$

Note that $|\omega_{*e} - \omega_{*i}|$ can be expressed as $|\omega_{*e}| + |\omega_{*i}|$.

The observed real frequencies for $T_i/T_e = 1.0$ are zero in accordance with the theory because $\omega_{*e}+\omega_{*i} = 0$. Also, the dependence of the measured growth rates on the $(|\omega_{*e}| + |\omega_{*i}|)/(2\gamma_0)$ agrees very well with the theory; γ reduces drastically as the density gradient increases. However very weak instability remains for $|\omega_{*e}| + |\omega_{*i}| > 2\gamma_0$. This residual instability will be discussed at the end of this section.

It is interesting to recognize the difference between the models which are valid for whole values of $k_\perp \rho_{ti}$ and valid only for long wavelength limit of $k_\perp \rho_{ti}$. When the vortex equation which is valid only for small value of $k_\perp \rho_{ti}$ is used, we have the growth rates and angular frequencies which are shown in Fig.2. The dispersion relation for the formula which is valid for the long wavelength,

$$\omega^2(\omega - \omega_{*i})(\omega - \omega_{*e})^3 = (i\gamma_0)^6 , \quad (34)$$

is obtained by the matching method (for example see [22]) and displayed in Fig.2 by numerically solving Eq.(34). Both dispersion relations (Eqs.(28) and (34)) are the same in the limit of $T_i = 0$. The simulation results for the model valid for long wavelength agree quite well with the theory in the same limit. The theoretical predictions of the growth rate for $T_i/T_e = 0$ and $T_i/T_e = 1$, which is valid for whole value of $k_\perp \rho_{ti}$, are also shown in Fig.2. We find that the ion diamagnetic effect is weak for the long wavelength model. The growth rate is somewhat close to the theoretical curve for $T_i/T_e = 0$. The eigenmode pattern rotates in the electron diamagnetic direction whereas the magnitude of the electron and ion diamagnetic drifts are the same for $T_i/T_e = 1$.

The data which will be shown hereafter are obtained by using the model which is valid for the whole

rage of $k_\perp \rho_{ti}$. Figure 3 shows the growth rates versus T_i/T_e. When there is no density gradient ($\epsilon_n = 0$), the growth rate increases with the ion temperature which is consistent with the theory. For the case with the density gradient of $\epsilon_n = 0.07071$, the growth rate enhances slightly with the ion temperature for the lower value of T_i/T_e, while for the higher value of T_i/T_e the growth rate reduces with the ion temperature. The amount of the reduction from the curve with $\epsilon_n = 0$ to the curve with $\epsilon_n = 0.07071$ corresponds to the stabilization of the mode by the electron and ion diamagnetic effects.

Figure 4 displays the angular frequencies versus T_i/T_e for the cases of $\epsilon_n = 0$ and $\epsilon_n = 0.07071$. There are poloidal rotations of the eigenmode patterns corresponding to the respective angular frequencies. The observed angular frequency is zero for the case of uniform density. The case with the density gradient is summarized as follows. When T_i/T_e is less than unity, the mode rotates in the electron diamagnetic direction. With $T_i/T_e = 1$ no poloidal rotation is observed. The mode rotates in the ion diamagnetic direction when $T_i/T_e > 1$. These results agree with the theory in which $\omega_r \propto T_i/T_e - 1$ (Eq.(30)).

The typical mode pattern of the unstable $m = 1$ kink mode for the uniform density is observed in Fig.5 which shows the profiles of ϕ and perturbed J_e (δJ_e) around the $q = 1$ surface in the (r, θ) coordinates. Note the difference in the scale of the horizontal axis of $(r - r_0)/a$ for ϕ and δJ_e. The perturbed current profile is localized at the rational surface and has the characteristic scale length of d_e which is much less than the characteristic scale lengths of ρ_s and ρ_{ti} of the potential profile. The case of $T_i/T_e = 0$ (Fig.5(a)) is compared with the case of $T_i/T_e = 1$ (Fig.5(b)). The mode pattern of the potential with $T_i/T_e = 1$ has the fine structure near the rational surface; the mode profile has the drastic change between $\Delta r < \rho_{ti}$ and $\Delta r > \rho_{ti}$ where Δr is the distance from the rational surface. This drastic change of the potential profile reflects the treatment of ion diamagnetic effects which are valid for the whole values of $k_\perp \rho_{ti}$.

The mode patterns of ϕ and δJ_e with the density gradient of $\epsilon_n = 0.07071$ for the different value of the temperature are shown in Fig.6. Fig.6(a) shows the case with $T_i/T_e = 0$. The mode pattern rotates in the electron diamagnetic direction. As the electron diamagnetic term becomes zero just at the rational surface ($k_\parallel = 0$), there is an effective shear in the electron diamagnetic effects. Hence the mode pattern experiences the V-shape deformation.

The case of $T_i/T_e = 1$ is shown in Fig.6(b). Although no diamagnetic rotation is observed by the cancellation of electron and ion diamagnetic drifts. The mode structures are influenced by the both diamagnetic effects. The case of $T_i/T_e = 2$ in which the mode pattern moves in the ion diamagnetic effect is shown in Fig.6(c).

Here, we return to the case of $T_i/T_e = 1$ and discuss the origin of the residual instability shown in Fig.1. Note that the theories predict complete stabilization for $|\omega_{*e}| + |\omega_{*i}| > 2\gamma_0$. Figure 7(a) shows the potential profile around the $q = 1$ surface for $\epsilon_n = 0.1187$ ($(|\omega_{*e}| + |\omega_{*i}|)/(2\gamma_0) = 1.008$) which is very close to the theoretical limit of $|\omega_{*e}| + |\omega_{*i}| = 2\gamma_0$. This case corresponds to the data designated by the letter A in Fig.1. We can see that the drift-wave like mode propagates into the outer regions (to the magnetic axis and to the plasma surface) from the rational surface. This mode pattern is observed only in the electrostatic potential; so the mode is essentially electrostatic. The density gradient broadens the characteristic length of the potential profile; the width of the zone of drift-wave like mode pattern becomes much larger than ρ_s and ρ_{ti}. The stabilization mechanism is expected that the energy of the unstable kink mode is extracted from the thin inertial layer to the outer regions.

Figure 7(b) shows the potential profile around the rational surface for $\epsilon_n = 0.1697$ ($(|\omega_{*e}| + |\omega_{*i}|)/(2\gamma_0) = 1.443$). This case is denoted by the letter B in Fig.1. The radial extent of the potential perturbation becomes large as the density gradient increases. We can see that the area where the drift-wave like mode can propagate is limited to the region with the density gradient. So if there are not enough spaces for the shear damping of the drift-wave like mode, the wave will reflected back to the rational surface. The spatial structure of the drift-wave like mode exhibits the mode pattern of the standing waves due to the mode coupling between outgoing and reflected waves.

Up to this place l_n has been fixed as 0.16. Here, the case of $l_n = 0.08$ with $\epsilon_n = 0.08485$ is shown in Fig.7(c). The parameter, $(|\omega_{*e}| + |\omega_{*i}|)/(2\gamma_0)$, is the same as that of Fig.7(b). The measured widths of the broadening of the mode pattern by the density gradient are limited by $\simeq l_n$ supporting the above mentioned speculation.

5 Conclusions and Discussion

Effects of density gradients on the $m = 1$ and $n = 1$ kinetic internal kink mode are studied numerically by the linearized version of GRM3F-CY code which is the three-field gyro-reduced-MHD code in the cylindrical geometry. While the previous paper [7] treated the electron diamagnetic effects in the limit of $T_i = 0$, the ion diamagnetic effects are investigated in this article. The gyro-reduced-MHD equations with the ion diamagnetic effects are obtained from the gyrokinetic Vlasov-Maxwell system given by Hahm [13]. It is found that the basic equations in the long wavelength limit of $k_\perp \rho_{ti} \ll 1$ fails to constitute the valid dispersion relation for the internal kink mode. The formulation valid even for $k_\perp \rho_{ti} \gg 1$ is necessary. The term $1 - \Gamma_0(k_\perp^2 \rho_{ti}^2)$ is the origin of the finite gyroradius effects of ions. The Padé like approximation, $1 - \Gamma_0 \simeq k_\perp^2 \rho_{ti}^2/(1 + k_\perp^2 \rho_{ti}^2)$, is used to make the code in the framework of the finite difference method. Final equations are very close to the subset of the four field model of Aydemir [15]. Hence, the Padé like approximation bridges the gap between the fluid equations

obtained from the gyrokinetic model and the standard kinetic model.

In order to resolve the mode structure with the characteristic lengths of d_e, ρ_s, and ρ_{ti} in the realistic parameters of present day large tokamaks, GRM3F-CY accumulates meshes around the $q = 1$ rational surface. We have selected $d_e = 5.315 \times 10^{-4}$ and $\rho_s = 2.891 \times 10^{-3}$. The ion diamagnetic effect is controlled by changing the parameter of T_i/T_e. The results of numerical calculation coincide with the theory for $|\omega_{*e}| + |\omega_{*i}| < 2\gamma_0$, where the growth rate reduces as the density gradient increases. Here γ_0 is the growth rate for the uniform density. Very weak instability, however, is observed for $|\omega_{*e}|+|\omega_{*i}| > 2\gamma_0$, where theories predict the complete stabilization.

One explanation of the stabilization of the kinetic internal kink mode is the energy extraction from the unstable region by the drift-wave like mode. The stabilization is, hence, effective only if there is a sufficient space around the $q = 1$ rational surface so that the drift-wave like mode can propagate in the radial directions. The observed residual instability may be excited since the region with the density gradient is limited in the radial direction and the stabilization by the outgoing drift-wave like mode becomes incomplete. Although ion Landau damping was not included in this study, it may be possible that the inclusion of ion Landau damping may increase the stabilizing effects of the drift-wave like mode propagating outside of the $q = 1$ surface.

As discussed in the previous paper [7], it will be interesting to study the nonlinear behavior of the residual instability, since this instability has both characteristics of the electrostatic drift wave and the internal kink mode. Also, the nonlinear stabilization of the kinetic internal kink mode which is linearly unstable is the subject of our investigation. Thus the development of the nonlinear version of GRM3F-CY code is our project in the near future.

Acknowledgement

The authors are grateful to Professor Osamu Fukumasa, Yamaguchi University, Drs. M. Azumi and Y. Kishimoto, JAERI, Professors T. Sato, T. Kamimura, and K. Itoh, National Institute for Fusion Science, Professor M. Wakatani, Kyoto University, and Professor S.I. Itoh, Research Institute for Applied Mechanics, Kyushu University for supporting their works. This work is partly supported by the collaboration programme of Japan Atomic Energy Research Institute, National Institute for Fusion Science, and Research Institute for Applied Mechanics, Kyushu University.

References

[1] H. Naitou, K. Tsuda, W.W. Lee, and R.D. Sydora, Phys. Plasmas **2**, 4257 (1995).

[2] H. Naitou, T. Sonoda, S. Tokuda, and V.K. Decyk, Journal of Plasma and Fusion Research **72**, 259 (1996).

[3] T. Matsumoto, S Tokuda, Y Kishimoto, T Takizuka, H. Naitou, Journal of Plasma and Fusion Research **75**, 1188 (1999).

[4] H. Naitou, H. Kitagawa, S. Tokuda, Journal of Plasma and Fusion Research **73**, 174 (1997).

[5] H. Naitou, T. Kobayashi, S Tokuda, J. Plasma Physics **61**, 543 (1999).

[6] S. Tokuda, H. Naitou, W.W. Lee, Journal of Plasma and Fusion Research **74**, 44 (1998).

[7] H. Naitou, T. Kobayashi, T. Kuramoto, S. Tokuda, T. Matsumoto, J. Plasma Fusion Research SERIES **2**, 259 (1999).

[8] F. Porcelli, Phys. Rev. Lett. **28**, 425 (1991).

[9] A.Y. Aydemir, Phys. Fluids **B4**, 3469 (1992).

[10] L. Zakharov, B. Rogers, Phys. Fluids B **4**, 3285 (1992).

[11] L. Zakharov, B. Rogers, S. Migliuolo, Phys. Fluids B **5**, 2498 (1993).

[12] W.W. Lee, reports presented at US-Japan Workshop on Plasma Modeling with MHD and Particle Simulation, Sep.25-26, 161(1987).

[13] T.S. Hahm, W.W. Lee, and A. Brizard, Phys. Fluids **31**, 1940 (1988).

[14] H. R. Strauss, Phys. Fluids **19**, 134 (1976).

[15] A.Y. Aydemir, Phys. Fluids B **3** . 3025 (1991).

[16] R.D. Hazeltine, C.T. Hsu, J. Morrison Phys. Fluids **30**, 3204 (1987).

[17] W. Dorland, G.W. Hamett, Phys. Fluids B **5**, 812 (1993).

[18] S. Chandrasekhar, "Hydrodynamic and Hydromagnetic Stability", Dover Publications, Inc., New York, 16 (1981).

[19] A. Hasegawa, L. Chen, Phys. Fluids **19**, 1924 (1976).

[20] A. Hasegawa, M. Wakatani, Phys. Fluids **26**, 2770 (1983).

[21] G.W. Hammett, W. Dorland, F.W. Perkins, Phys. Fluids B **4**, 2052 (1992).

[22] T.S. Hahm, Ph. D. thesis, Princeton University (1984).

Figure captions

Fig.1 The normalized growth rate γ/γ_0 versus $(|\omega_{*e}| + |\omega_{*i}|)/(2\gamma_0)$ for $T_i/T_e = 1.0$. The basic equations are valid for all value of $k_\perp \rho_{ti}$. The theoretical curve written in the figure is $\gamma/\gamma_0 = \sqrt{1 - [(|\omega_{*e}| + |\omega_{*i}|)/(2\gamma_0)]^2}$.

Fig.2 The normalized growth rate and angular frequency for $T_i/T_e = 1.0$ depending on ω_{*e}/γ_0. The basic equations are valid only for long wavelength limit of $k_\perp \rho_{ti}$. The theory for the long wavelength model is shown in the figure. The curves for the growth rate for $T_i/T_e = 0$ and $T_i/T_e = 1.0$ are obtained by the theory being valid for the whole range of $k_\perp \rho_{ti}$.

Fig.3 The growth rates versus T_i/T_e for $\epsilon_n = 0$ and $\epsilon_n = 0.07071$.

Fig.4 The angular frequencies versus T_i/T_e for $\epsilon_n = 0$ and $\epsilon_n = 0.07071$. For the positive value of ω_r the mode pattern rotates in the ion diamagnetic direction, while for the negative value it rotates in the electron diamagnetic direction.

Fig.5 The contour plot of ϕ and perturbed J_e around the $q = 1$ magnetic surface at $r = 0.5a$ in the $r - \theta$ coordinates. The cases without the density gradient are shown. (a) $T_i/T_e = 0$ and (b) $T_i/T_e = 1$,

Fig.6 The contour plot of ϕ and perturbed J_e around the $q = 1$ magnetic surface at $r = 0.5a$ in the $r-\theta$ coordinates. The cases with the density gradient of $\epsilon_n = 0.07071$ are shown. (a) $T_i/T_e = 0$, (b) $T_i/T_e = 1$, and (c) $T_i/T_e = 2$.

Fig.7 The contour plots of ϕ around the $q = 1$ magnetic surface at $r = 0.5a$ in the $r - \theta$ coordinates for (a)$\epsilon_n = 0.1187$ and $l_n/a = 0.16$, (b)$\epsilon_n = 0.1697$ and $l_n/a = 0.16$, and (c)$\epsilon_n = 0.08485$ and $l_n/a = 0.08$.

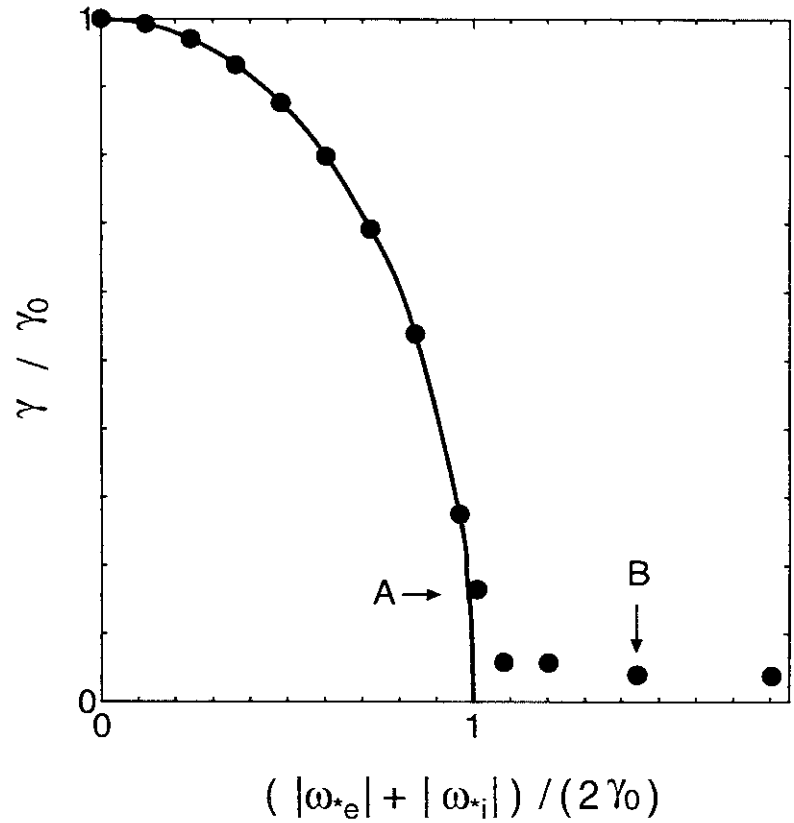
γ / γ0
1
0
0
1
A
B
(|ω*e| + | ω*i|) / (2 γ0)

Fig.1

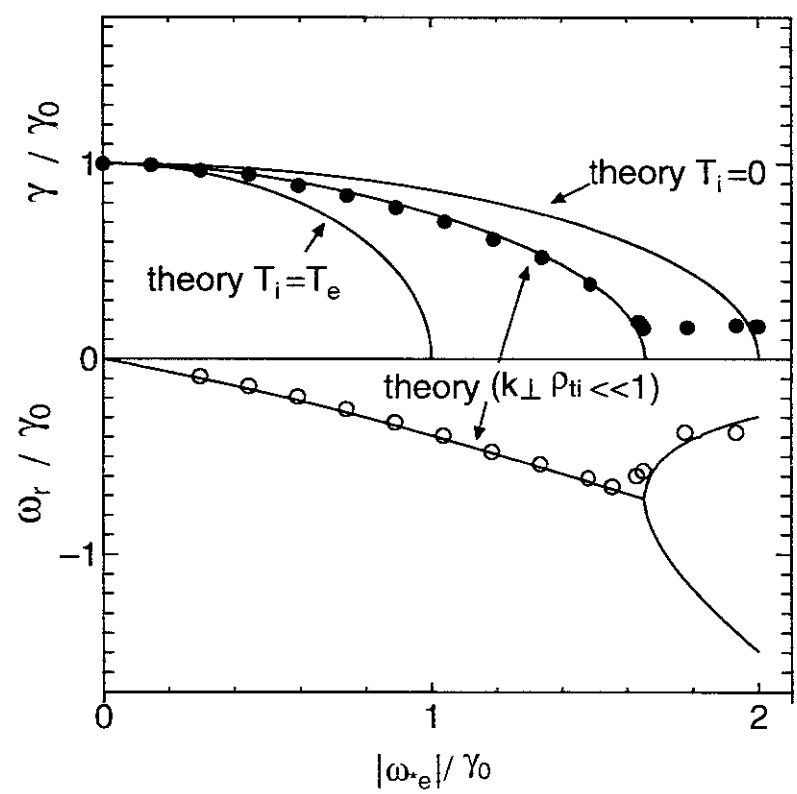
γ / γ0
1
0
theory Ti=0
theory Ti=Te
theory (k⊥ ρti <<1)
ωr / γ0
−1
0
1
2
|ω*e|/ γ0

Fig.2

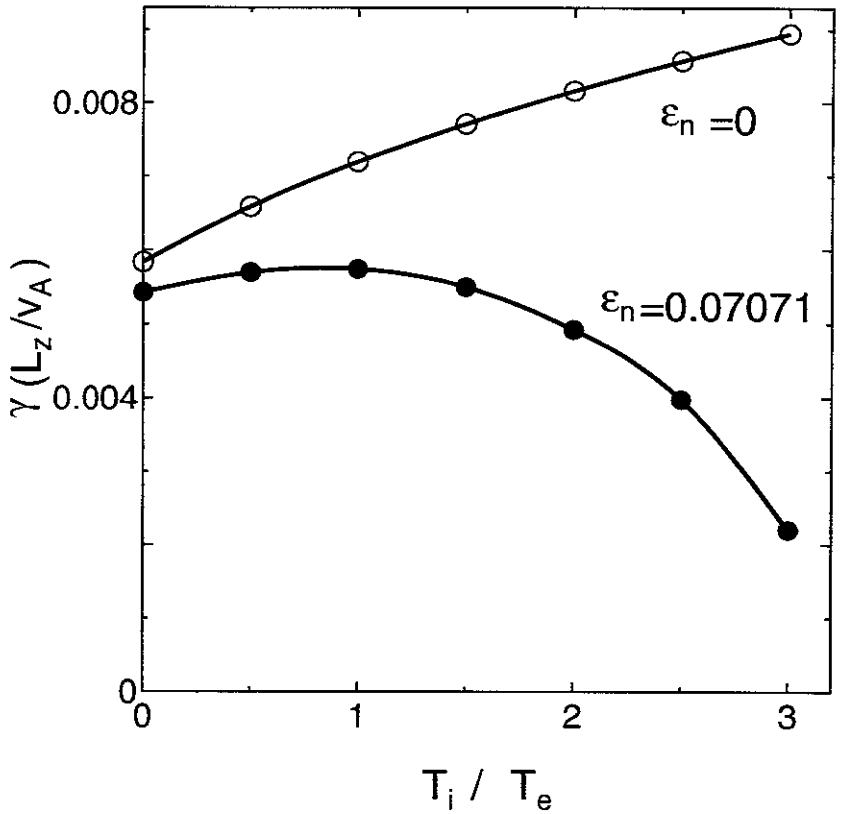
0.008
0.004
0
0
1
2
3
γ (L_z/v_A)
ε_n =0
ε_n=0.07071
T_i / T_e

Fig.3

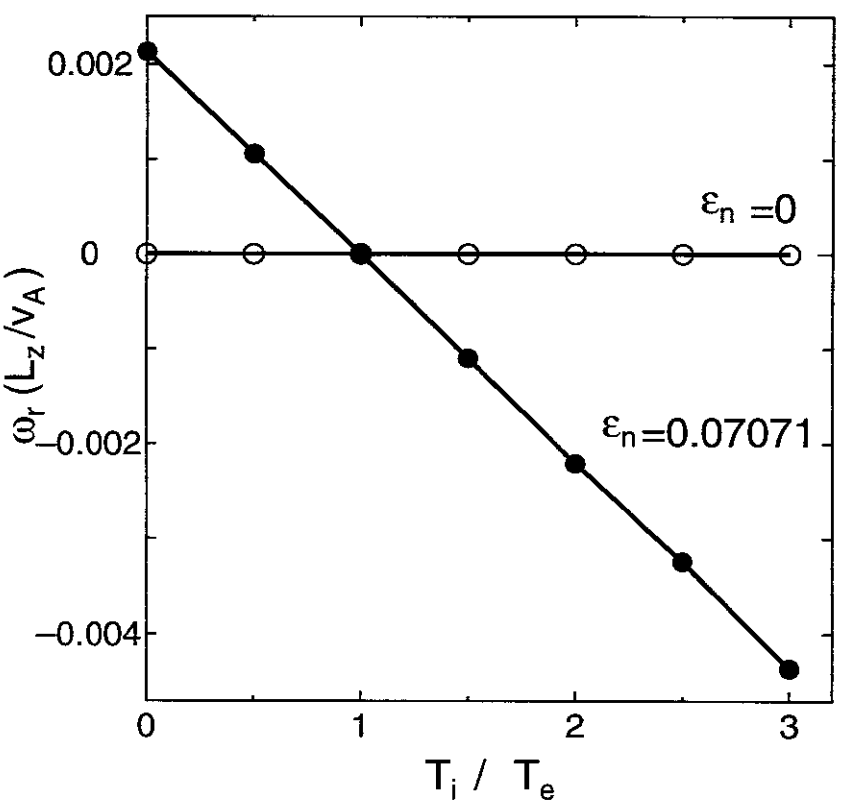
0.002
0
−0.002
−0.004
0
1
2
3
ω_r (L_z/v_A)
ε_n =0
ε_n=0.07071
T_i / T_e

Fig.4

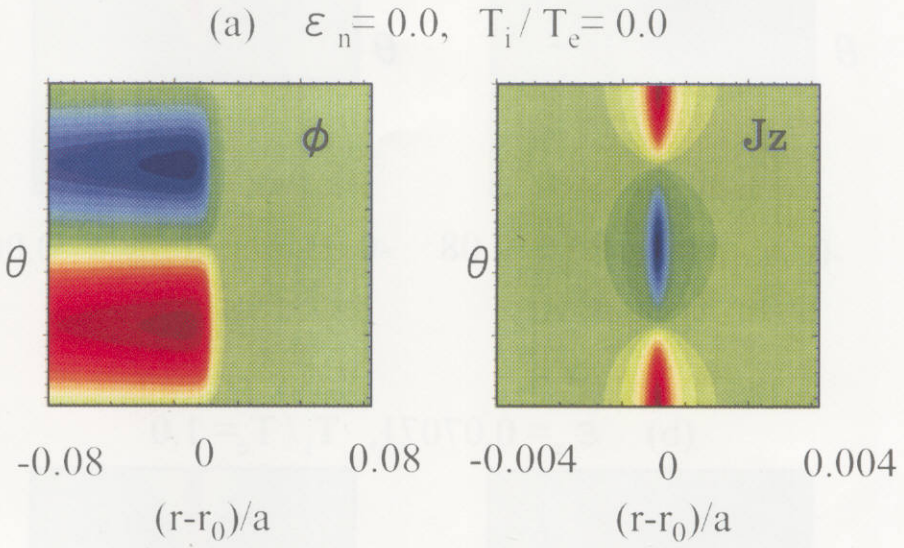
(a) $\varepsilon_n = 0.0$, $T_i / T_e = 0.0$
ϕ
Jz
θ
θ
-0.08
0
0.08
-0.004
0
0.004
$(r-r_0)/a$
$(r-r_0)/a$
(b) $\varepsilon_n = 0.0$, $T_i / T_e = 1.0$
ϕ
Jz
θ
θ
-0.08
0
0.08
-0.004
0
0.004
$(r-r_0)/a$
$(r-r_0)/a$

Fig.5

(a) $\varepsilon_n = 0.07071$, $T_i / T_e = 0.0$

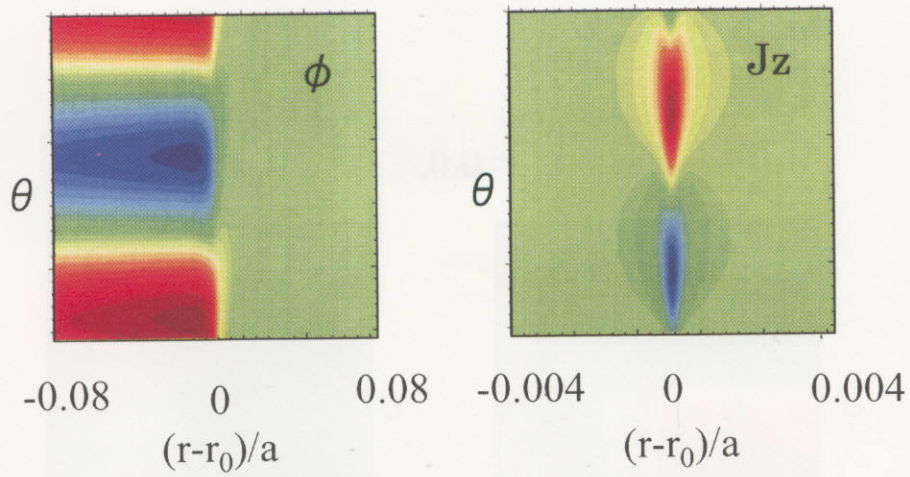

(b) $\varepsilon_n = 0.07071$, $T_i / T_e = 1.0$

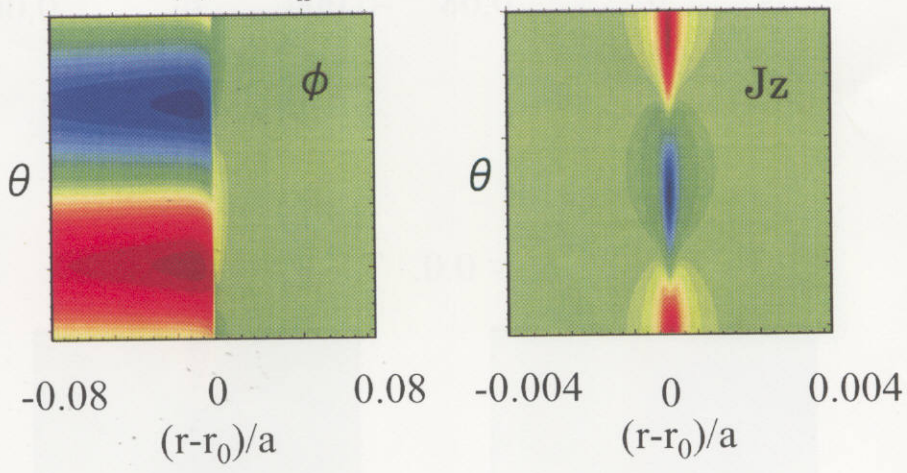

(c) $\varepsilon_n = 0.07071$, $T_i / T_e = 2.0$

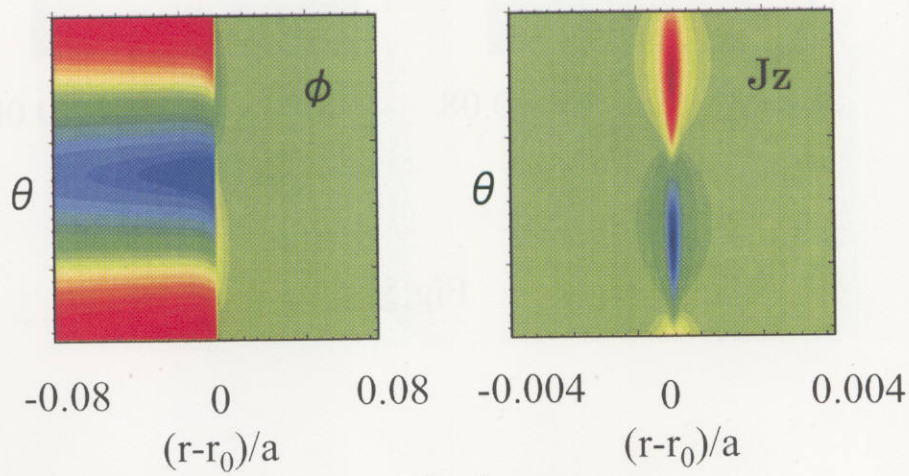

Fig.6

(a) $\varepsilon_n = 0.1187,\ l_n = 0.16$

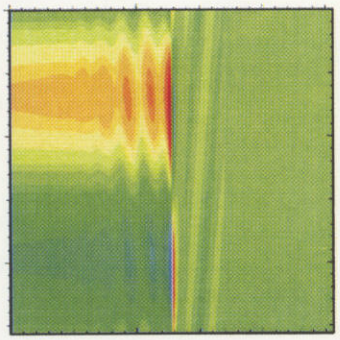

(b) $\varepsilon_n = 0.1697,\ l_n = 0.16$

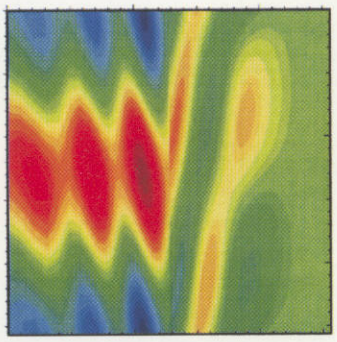

(c) $\varepsilon_n = 0.08485,\ l_n = 0.08$

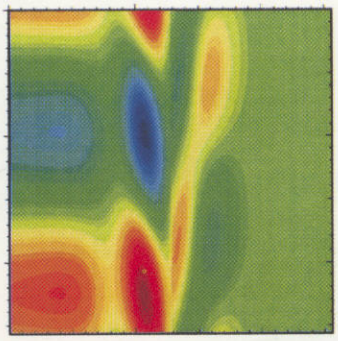

Fig.7

Recent Issues of NIFS Series

NIFS-569 M M Skoric, T Sato, A Maluckov, M S Jovanovic,
Micro- and Macro-scale Self-organization in a Dissipative Plasma, Oct 1998

NIFS-570 T Hayashi, N Mizuguchi, T-H Watanabe, T Sato and the Complexity Simulation Group,
Nonlinear Simulations of Internal Reconnection Event in Spherical Tokamak; Oct 1998
(IAEA-CN-69/TH3/3)

NIFS-571 A Iiyoshi, A Komori, A Ejiri, M Emoto, H Funaba, M Goto, K Ida, H Idei, S Inagaki, S Kado, O Kaneko, K Kawahata, S Kubo, R Kumazawa, S Masuzaki, T Minami, J Miyazawa, T Morisaki, S Morita, S Murakami, S Muto, T Muto, Y Nagayama, Y Nakamura, H Nakanishi, K Narihara, K Nishimura, N Noda, T Kobuchi, S Ohdachi, N Ohyabu, Y Oka, M Osakabe, T Ozaki, B J Peterson, A Sagara, S Sakakibara, R Sakamoto, H Sasao, M Sasao, K Sato, M Sato, T Seki, T Shimozuma, M Shoji, H Suzuki, Y Takeiri, K Tanaka, K Toi, T Tokuzawa, K Tsumori, I Yamada, H Yamada, S Yamaguchi, M Yokoyama, K Y Watanabe, T Watari, R Akiyama, H Chikaraishi, K Haba, S Hamaguchi, S Iima, S Imagawa, N Inoue, K Iwamoto, S Kitagawa, Y Kubota, J Kodaira, R Maekawa, T Mito T Nagasaka, A Nishimura, Y Takita, C Takahashi, K Takahata, K Yamauchi, H Tamura, T Tsuzuki, S Yamada, N Yanagi, H Yonezu, Y Hamada, K Matsuoka, K Murai, K Ohkubo, I Ohtake, M Okamoto, S Sato, T Satow, S Sudo, S Tanahashi, K Yamazaki, M Fujiwara and O Motojima,
An Overview of the Large Helical Device Project; Oct 1998
(IAEA-CN-69/OV1/4)

NIFS-572 M. Fujiwara, H. Yamada, A. Ejiri, M Emoto, H Funaba, M. Goto, K. Ida, H Idei, S. Inagaki, S. Kado, O. Kaneko, K Kawahata, A Komori, S. Kubo, R. Kumazawa, S. Masuzaki, T. Minami, J. Miyazawa, T Morisaki, S. Morita, S. Murakami, S Muto, T. Muto, Y Nagayama, Y. Nakamura, H. Nakanishi, K. Narihara, K Nishimura, N. Noda, T Kobuchi, S. Ohdachi, N. Ohyabu, Y. Oka, M Osakabe, T. Ozaki, B. J. Peterson, A. Sagara, S. Sakakibara, R. Sakamoto, H. Sasao, M. Sasao, K Sato, M. Sato, T Seki, T. Shimozuma, M. Shoji, H Sazuki, Y. Takeiri, K Tanaka, K Toi, T Tokuzawa, K. Tsumori, I Yamada, S. Yamaguchi, M Yokoyama, K.Y. Watanabe, T. Watari, R. Akiyama, H Chikaraishi, K Haba, S. Hamaguchi, M. Iima, S. Imagawa, N. Inoue, K. Iwamoto, S Kitagawa, Y. Kubota, J. Kodaira, R Maekawa, T Mito, T. Nagasaka, A. Nishimura, Y Takita, C Takahashi, K. Takahata, K. Yamauchi, H. Tamura, T. Tsuzuki, S. Yamada, N. Yanagi, H Yonezu, Y. Hamada, K. Matsuoka, K. Murai, K. Ohkubo, I. Ohtake, M Okamoto, S. Sato, T Satow, S. Sudo, S. Tanahashi, K. Yamazaki, O Motojima and A. Iiyoshi,
Plasma Confinement Studies in LHD, Oct 1998
(IAEA-CN-69/EX2/3)

NIFS-573 O Motojima, K. Akaishi, H. Chikaraishi, H. Funaba, S. Hamaguchi, S. Imagawa, S. Inagaki, N. Inoue, A. Iwamoto, S. Kitagawa, A. Komori, Y Kubota, R. Maekawa, S Masuzaki, T Mito, J Miyazawa, T Morisaki, T Muroga, T. Nagasaka, Y. Nakmura, A. Nishimura, K. Nishimura, N. Noda, N. Ohyabu, S. Sagara, S Sakakibara, R. Sakamoto, S Satoh, T. Satow, M. Shoji, H. Suzuki, K Takahata, H. Tamura, K Watanabe, H. Yamada, S Yamada, S. Yamaguchi, K Yamazaki, N. Yanagi, T. Baba, H. Hayashi, M. Iima, T. Inoue, S. Kato, T. Kato, T. Kondo, S. Moriuchi, H. Ogawa, I Ohtake, K Ooba, H Sekiguchi, N. Suzuki, S Takami, Y. Taniguchi, T. Tsuzuki, N. Yamamoto, K Yasui, H. Yonezu, M. Fujiwara and A Iiyoshi,
Progress Summary of LHD Engineering Design and Construction; Oct 1998
(IAEA-CN-69/FT2/1)

NIFS-574 K Toi, M. Takechi, S. Takagi, G. Matsunaga, M. Isobe, T Kondo, M Sasao, D.S. Darrow, K Ohkuni, S. Ohdachi, R. Akiyama A Fujisawa, M. Gotoh, H. Idei, K Ida, H Iguchi, S. Kado, M. Kojima, S. Kubo, S. Lee, K Matsuoka, T. Minami, S. Morita, N Nikai, S. Nishimura, S. Okamura, M Osakabe, A Shimizu, Y Shirai, C Takahashi, K Tanaka, T. Watari and Y. Yoshimura,
Global MHD Modes Excited by Energetic Ions in Heliotron/Torsatron Plasmas; Oct. 1998
(IAEA-CN-69/EXP1/19)

NIFS-575 Y Hamada, A Nishizawa, Y. Kawasumi, A Fujisawa, M. Kojima, K Narihara, K Ida, A Ejiri, S Ohdachi, K Kawahata, K Toi, K Sato, T. Seki, H. Iguchi, K Adachi, S. Hidekuma, S Hirokura, K Iwasaki, T Ido, R. Kumazawa, H. Kuramoto, T. Minami, I. Nomura, M. Sasao, K.N. Sato, T Tsuzuki, I Yamada and T Watari,
Potential Turbulence in Tokamak Plasmas, Oct. 1998
(IAEA-CN-69/EXP2/14)

NIFS-576 S Murakami, U. Gasparino, H. Idei, S. Kubo, H Maassberg, N Marushchenko, N Nakajima, M Romé and M. Okamoto,
5D Simulation Study of Suprathermal Electron Transport in Non-Axisymmetric Plasmas; Oct 1998
(IAEA-CN-69/THP1/01)

NIFS-577 S Fujiwara and T Sato,
Molecular Dynamics Simulation of Structure Formation of Short Chain Molecules; Nov. 1998

NIFS-578 T Yamagishi,
Eigenfunctions for Vlasov Equation in Multi-species Plasmas Nov. 1998

NIFS-579 M. Tanaka, A Yu Grosberg and T Tanaka,
Molecular Dynamics of Strongly-Coupled Multichain Coulomb Polymers in Pure and Salt Aqueous Solutions, Nov. 1998

NIFS-580 J Chen, N Nakajima and M Okamoto,
Global Mode Analysis of Ideal MHD Modes in a Heliotron/Torsatron System: I. Mercier-unstable Equilibria; Dec 1998

NIFS-581 M. Tanaka, A. Yu Grosberg and T Tanaka,
Comparison of Multichain Coulomb Polymers in Isolated and Periodic Systems: Molecular Dynamics Study; Jan. 1999

NIFS-582 V.S. Chan and S. Murakami,
Self-Consistent Electric Field Effect on Electron Transport of ECH Plasmas; Feb. 1999

NIFS-583 M. Yokoyama, N. Nakajima, M. Okamoto, Y. Nakamura and M. Wakatani,
Roles of Bumpy Field on Collisionless Particle Confinement in Helical-Axis Heliotrons; Feb. 1999

NIFS-584 T.-H. Watanabe, T. Hayashi, T. Sato, M. Yamada and H. Ji,
Modeling of Magnetic Island Formation in Magnetic Reconnection Experiment; Feb. 1999

NIFS-585 R. Kumazawa, T Mutoh, T. Seki, F Shinpo, G. Nomura, T Ido, T. Watari, Jean-Marie Noterdaeme and Yangping Zhao,
Liquid Stub Tuner for Ion Cyclotron Heating, Mar 1999

NIFS-586 A. Sagara, M. Iima, S. Inagaki, N. Inoue, H. Suzuki, K. Tsuzuki, S. Masuzaki, J. Miyazawa, S. Morita, Y. Nakamura, N. Noda, B. Peterson, S. Sakakibara, T. Shimozuma, H. Yamada, K. Akaishi, H. Chikaraishi, H. Funaba, O. Kaneko, K. Kawahata, A. Komori, N. Ohyabu, O. Motojima, LHD Exp. Group 1, LHD Exp. Group 2,
Wall Conditioning at the Starting Phase of LHD; Mar. 1999

NIFS-587 T. Nakamura and T. Yabe,
Cubic Interpolated Propagation Scheme for Solving the Hyper-Dimensional Vlasov-Poisson Equation in Phase Space; Mar 1999

NIFS-588 W.X. Wnag, N. Nakajima, S. Murakami and M. Okamoto,
An Accurate δf Method for Neoclassical Transport Calculation, Mar 1999

NIFS-589 K. Kishida, K. Araki, S. Kishiba and K. Suzuki,
Local or Nonlocal? Orthonormal Divergence-free Wavelet Analysis of Nonlinear Interactions in Turbulence; Mar. 1999

NIFS-590 K. Araki, K. Suzuki, K. Kishida and S. Kishiba,
Multiresolution Approximation of the Vector Fields on T^3; Mar. 1999

NIFS-591 K. Yamazaki, H. Yamada, K.Y.Watanabe, K. Nishimura, S. Yamaguchi, H. Nakanishi, A. Komori, H. Suzuki, T. Mito, H. Chikaraishi, K. Murai, O. Motojima and the LHD Group,
Overview of the Large Helical Device (LHD) Control System and Its First Operation; Apr. 1999

NIFS-592 T. Takahashi and Y. Nakao,
Thermonuclear Reactivity of D-T Fusion Plasma with Spin-Polarized Fuel; Apr. 1999

NIFS-593 H. Sugama,
Damping of Toroidal Ion Temperature Gradient Modes; Apr. 1999

NIFS-594 Xiaodong Li,
Analysis of Crowbar Action of High Voltage DC Power Supply in the LHD ICRF System; Apr 1999

NIFS-595 K. Nishimura, R. Horiuchi and T Sato,
Drift-kink Instability Induced by Beam Ions in Field-reversed Configurations; Apr. 1999

NIFS-596 Y. Suzuki, T-H. Watanabe, T. Sato and T Hayashi,
Three-dimensional Simulation Study of Compact Toroid Plasmoid Injection into Magnetized Plasmas; Apr. 1999

NIFS-597 H. Sanuki, K. Itoh, M. Yokoyama, A. Fujisawa, K. Ida, S. Toda, S.-I Itoh, M. Yagi and A. Fukuyama,
Possibility of Internal Transport Barrier Formation and Electric Field Bifurcation in LHD Plasma; May 1999

NIFS-598 S. Nakazawa, N. Nakajima, M. Okamoto and N. Ohyabu,
One Dimensional Simulation on Stability of Detached Plasma in a Tokamak Divertor; June 1999

NIFS-599 S. Murakami, N. Nakajima, M. Okamoto and J. Nhrenberg,
Effect of Energetic Ion Loss on ICRF Heating Efficiency and Energy Confinement Time in Heliotrons;

June 1999

NIFS-600 R. Horiuchi and T. Sato,
Three-Dimensional Particle Simulation of Plasma Instabilities and Collisionless Reconnection in a Current Sheet,, June 1999

NIFS-601 W. Wang, M. Okamoto, N. Nakajima and S. Murakami,
Collisional Transport in a Plasma with Steep Gradients, June 1999

NIFS-602 T. Mutoh, R. Kumazawa, T. Saki, K. Saito, F. Simpo, G. Nomura, T. Watari, X. Jikang, G. Cattanei, H. Okada, K. Ohkubo, M. Sato, S. Kubo, T. Shimozuma, H. Idei, Y. Yoshimura, O. Kaneko, Y. Takeiri, M. Osakabe, Y. Oka, K. Tsumori, A. Komori, H. Yamada, K. Watanabe, S. Sakakibara, M. Shoji, R. Sakamoto, S. Inagaki, J. Miyazawa, S. Morita, K. Tanaka, B.J. Peterson, S. Murakami, T. Minami, S. Ohdachi, S. Kado, K. Narihara, H. Sasao, H. Suzuki, K. Kawahata, N. Ohyabu, Y. Nakamura, H. Funaba, S. Masuzaki, S. Muto, K. Sato, T. Morisaki, S. Sudo, Y. Nagayama, T. Watanabe, M. Sasao, K. Ida, N. Noda, K. Yamazaki, K. Akaishi, A. Sagara, K. Nishimura, T. Ozaki, K. Toi, O. Motojima, M. Fujiwara, A. Iiyoshi and LHD Exp. Group 1 and 2,
First ICRF Heating Experiment in the Large Helical Device, July 1999

NIFS-603 P.C. de Vries, Y. Nagayama, K. Kawahata, S. Inagaki, H. Sasao and K. Nagasaki,
Polarization of Electron Cyclotron Emission Spectra in LHD, July 1999

NIFS-604 W. Wang, N. Nakajima, M. Okamoto and S. Murakami,
δf Simulation of Ion Neoclassical Transport; July 1999

NIFS-605 T. Hayashi, N. Mizuguchi, T. Sato and the Complexity Simulation Group,
Numerical Simulation of Internal Reconnection Event in Spherical Tokamak; July 1999

NIFS-606 M. Okamoto, N. Nakajima and W. Wang,
On the Two Weighting Scheme for δf Collisional Transport Simulation, Aug. 1999

NIFS-607 O. Motojima, A.A. Shishkin, S. Inagaki, K.Y. Watanabe,
Possible Control Scenario of Radial Electric Field by Loss-Cone-Particle Injection into Helical Device; Aug. 1999

NIFS-608 R. Tanaka, T. Nakamura and T. Yabe,
Constructing Exactly Conservative Scheme in Non-conservative Form; Aug. 1999

NIFS-609 H. Sugama,
Gyrokinetic Field Theory, Aug. 1999

NIFS-610 M. Takechi, G. Matsunaga, S. Takagi, K.Ohkuni, K. Toi, M. Osakabe, M. Isobe, S. Okamura, K. Matsuoka, A. Fujisawa, H. Iguchi, S. Lee, T. Minami, K. Tanaka, Y. Yoshimura and CHS Group,
Core Localized Toroidal Alfven Eigenmodes Destabilized By Energetic Ions in the CHS Heliotron/Torsatron, Sep. 1999

NIFS-611 K. Ichiguchi,
MHD Equilibrium and Stability in Heliotron Plasmas, Sep. 1999

NIFS-612 Y. Sato, M. Yokoyama, M. Wakatani and V. D. Pusovitov,
Complete Suppression of Pfirsch-Schluter Current in a Toroidal l=3 Stellarator, Oct. 1999

NIFS-613 S. Wang, H. Sanuki and H. Sugama,
Reduced Drift Kinetic Equation for Neoclassical Transport of Helical Plasmas in Ultra-low Collisionality Regime; Oct. 1999

NIFS-614 J. Miyazawa, H. Yamada, K. Yasui, S. Kato, N., Fukumoto, M. Nagata and T. Uyama,
Design of Spheromak Injector Using Conical Accelerator for Large Helical Device; Nov. 1999

NIFS-615 M. Uchida, A. Fukuyama, K. Itoh, S.-I. Itoh and M. Yagi,
Analysis of Current Diffusive Ballooning Mode in Tokamaks, Dec. 1999

NIFS-616 M. Tanaka, A.Yu. Grosberg and T. Tanaka,
Condensation and Swelling Behavior of Randomly Charged Multichain Polymers by Molecular Dynamics Simulations; Dec. 1999

NIFS-617 S. Goto and S. Kida,
Sparseness of Nonlinear Coupling, Dec. 1999

NIFS-618 M.M. Skoric, T. Sato, A. Maluckov and M.S. Jovanovic,
; *Complexity in Laser Plasma Instabilities* Dec. 1999

NIFS-619 T.-H. Watanabe, H. Sugama and T. Sato,
Non-dissipative Kinetic Simulation and Analytical Solution of Three-mode Equations of Ion Temperature Gradient Instability; Dec. 1999

NIFS-620 Y. Oka, Y. Takeiri, Yu I Belchenko, M. Hamabe, O. Kaneko, K. Tsumori, M. Osakabe, E. Asano, T Kawamoto, R. Akiyama,
Optimization of Cs Deposition in the 1/3 Scale Hydrogen Negative Ion Source for LHD-NBI System ;Dec. 1999

NIFS-621 Yu.I. Belchenko, Y. Oka, O Kaneko, Y Takeiri, A. Krivenko, M. Osakabe, K Tsumori, E. Asano, T. Kawamoto, R. Akiyama,
Recovery of Cesium in the Hydrogen Negative Ion Sources, Dec 1999

NIFS-622 Y. Oka, O. Kaneko, K. Tsumori, Y. Takeiri, M. Osakabe, T. Kawamoto, E Asano, and R. Akiyama.
H- Ion Source Using a Localized Virtual Magnetic Filter in the Plasma Electrode: Type I LV Magnetic Filter: Dec. 1999

NIFS-623 M. Tanaka, S Kida, S. Yanase and G. Kawahara,
Zero-absolute-vorticity State in a Rotating Turbulent Shear Flow; Jan. 2000

NIFS-624 F. Leuterer, S. Kubo,
Electron Cyclotron Current Drive at $\omega \approx \omega_c$ with X-mode Launched from the Low Field Side; Feb 2000

NIFS-625 K Nishimura,
Wakefield of a Charged Particulate Influenced by Emission Process of Secondary Electrons; Mar. 2000

NIFS-626 K Itoh, M. Yagi, S.-I. Itoh, A. Fukuyama,
On Turbulent Transport in Burning Plasmas; Mar 2000

NIFS-627 K Itoh, S.-I. Itoh, L Giannone,
Modelling of Density Limit Phenomena in Toroidal Helical Plasmas; Mar. 2000

NIFS-628 K Akaishi, M. Nakasuga and Y. Funato,
True and Measured Outgassing Rates of a Vacuum Chamber with a Reversibly Absorbed Phase; Mar. 2000

NIFS-629 T. Yamagishi,
Effect of Weak Dissipation on a Drift Orbit Mapping; Mar. 2000

NIFS-630 S. Toda, S.-I, Itoh, M. Yagi, A. Fukuyama and K Itoh,
Spatial Structure of Compound Dither in L/H Transition, Mar 2000

NIFS-631 N. Ishihara and S. Kida,
Axial and Equatorial Magnetic Dipoles Generated in a Rotating Spherical Shell; Mar. 2000

NIFS-632 T. Kuroda, H. Sugama, R. Kanno and M. Okamoto,
Ion Temperature Gradient Modes in Toroidal Helical Systems; Apr. 2000

NIFS-633 V.D. Pustovitov,
Magnetic Diagnostics: General Principles and the Problem of Reconstruction of Plasma Current and Pressure Profiles in Toroidal Systems; Apr. 2000

NIFS-634 A.B. Mikhailovskii, S.V. Konovalov, V.D. Pustovitov and V.S. Tsypin,
Mechanism of Viscosity Effect on Magnetic Island Rotation, Apr. 2000

NIFS-635 H. Naitou, T. Kuramoto, T. Kobayashi, M. Yagi, S. Tokuda and T. Matsumoto,
Stabilization of Kinetic Internal Kink Mode by Ion Diamagnetic Effects; Apr. 2000